

### **3. CORE-LOG CORRELATIONS IN OCEANIC BASEMENT FROM HOLE 1105A ON THE SOUTHWEST INDIAN RIDGE<sup>1</sup>**

D. Jay Miller,<sup>2,4</sup> Gerardo J. Iturrino,<sup>3</sup> and Jennifer C. McGuire<sup>4</sup>

#### **ABSTRACT**

During a lull in hammer drill testing during Ocean Drilling Program Leg 179, Hole 1105A was cored to 158 mbsf on the Southwest Indian Ridge within ~1.3 km of Hole 735B. This coring operation resulted in not only high recovery (in excess of 80%) but in the collection of a suite of continuous downhole logging data. This combination allows the rare opportunity to demonstrate the utility of logging in hard rock environments. By using the core as a reference, we have been able to recognize specific Formation MicroScanner (FMS) image characteristics that represent different structural aspects of the core. Gabbro with disseminated oxide has a mottled appearance in the FMS images, and in foliated intervals, the attitude of the foliation can be determined from FMS orientation. We also present evidence of decreased and poorer quality core recovery from intervals that have resistivity characteristics indicative of intense fracturing and that certain lithologic units can have markedly different characteristics in the FMS record, improving estimates of interval thickness. This study shows that, at least for this expedition, the material sampled is consistently (albeit not universally) from the top of the cored interval, which varies in lithologic character on scales as small as a few centimeters. Therefore, the core recovered does not necessarily proportionally represent the cored interval. Reorientation of structural data measured on cores and on FMS images to paleomagnetic data indicates the direction of principle stress during the crystallization and deformation history of the Atlantis Bank was parallel to the Southwest Indian Ridge axis.

<sup>1</sup>Miller, D.J., Iturrino, G.J., and McGuire, J.C., 2003. Core-log correlations in oceanic basement from Hole 1105A on the Southwest Indian Ridge. *In* Casey, J.F., and Miller, D.J. (Eds.), *Proc. ODP, Sci. Results*, 179, 1–29 [Online]. Available from World Wide Web: <[http://www-odp.tamu.edu/publications/179\\_SR/VOLUME/CHAPTERS/SR179\\_03.PDF](http://www-odp.tamu.edu/publications/179_SR/VOLUME/CHAPTERS/SR179_03.PDF)>. [Cited YYYY-MM-DD]

<sup>2</sup>Ocean Drilling Program, Texas A&M University, 1000 Discovery Drive, College Station TX 77845-9547, USA. [miller@odpemail.tamu.edu](mailto:miller@odpemail.tamu.edu)

<sup>3</sup>Borehole Research Group, Lamont-Doherty Earth Observatory of Columbia University, PO Box 1000, 61 Route 9W, Palisades NY 10964, USA.

<sup>4</sup>Department of Geology and Geophysics, Texas A&M University, College Station TX 77845, USA.

Initial receipt: 27 October 2000

Acceptance: 16 June 2003

Web publication: 9 December 2003

Ms 179SR-016

## INTRODUCTION

In 1987, the Ocean Drilling Program (ODP) Leg 118 cored Hole 735B to 500 meters below seafloor (mbsf) on the Southwest Indian Ridge, some 1300 km southeast of Madagascar. The results of that expedition led to a new multileg proposal to reoccupy Hole 735B. Owing to the remote location of this site, this achievement would not be fully realized until 10 yr later, when ODP Leg 176 returned to this location and deepened Hole 735B in this gabbroic massif to in excess of 1500 m. The entire cored interval at this site is gabbro and appears, from all measurable and interpretable values, to represent an intact section of the lower ocean crust (Dick et al., 2000). Hole 735B is not the deepest hole ever drilled by ODP, but the continuous recovery in excess of 85% is unprecedented in oceanic hard rock coring and the snapshot of ocean lower crustal structure, petrology, and lithostratigraphy provided by this core remains as one of the greatest legacies of scientific ocean drilling.

Despite the importance of this core in providing us a window into the lower ocean crust, there is no mechanism whereby the cores recovered from Hole 735B can be completely and systematically reoriented relative to north. Therefore, all structural measurements made on the cores can be determined with certainty only in the core reference frame (Shipboard Scientific Party, 1999a). This reference frame is potentially (albeit not likely) biased by the assumption of uniform foliation dip direction because cores are routinely split to maximize the dip of foliation on the cut surface of the core. Additionally, even with 80%–90% recovery, each core represents a cored interval of ~5–10 m. The core is broken into pieces, usually on the order of 10–20 cm long, with broken surfaces that cannot be fitted together and represent intervals of no recovery. Whereas drilling parameters let us estimate where coring started and ended (within probably <50 cm), we cannot say with certainty what specific intervals within a 10-m cored interval the core recovered actually represents. ODP convention (see Shipboard Scientific Party, 1999a) is to shunt all pieces of the core to the top of the cored interval for curation purposes, but because the description of these cores is carried out on a centimeter scale and whole- and split-core measurements are also made on a centimeter scale, the error on the curated depth of these measurements may be far greater than the resolution of the measurements themselves.

Whereas the Formation MicroScanner (FMS) and other logging tools have proven to be immensely useful correlation tools throughout the history of ocean drilling, the instances of demonstrable utility of these tools in hard rock applications are rare (e.g., C  lerier et al., 1996). This is almost certainly not a reflection of how well the tools work but more a testament to how few holes have penetrated deeply enough into hard rock to allow logging and how few of those have remained unobstructed and stable long enough to permit logging runs. We simply have not used these tools often enough to fully evaluate their potential. Prior to Leg 176, the only deployment of the FMS in subseafloor gabbroic rock was a short (<40 m thick) interval logged during Leg 147 (Shipboard Scientific Party, 1993). FMS data were recorded in Hole 735B during Leg 176, but hole obstruction (900 m of pipe in the lower part of the hole) limited coverage to the upper few hundred meters. In addition, during FMS data acquisition, voltage saturation warnings were persistent, leading to speculation that the seawater in the borehole was

creating a favored conductive path, thus degrading the FMS data (Shipboard Scientific Party, 1999d).

Four methods of deriving oriented data sets on ODP hard rock cores or boreholes are discussed in C  lerier et al. (1996). The first of these methods includes an orientation system that integrates a scribe mark on the core, monitors core entry into the bit and bit depth, and incorporates a fluxgate magnetometer on the core barrel. The integration of these systems has been an impediment to development, so although the potential remains, no working system exists. A second possible method is using remanent magnetization to reorient pieces of core (e.g., Cannat and Pariso, 1991). A third method (as developed in C  lerier et al., 1996) is to pick features that represent resistivity contrast from FMS logging data and interpret those features in terms of regional geology. A final method that involves orienting pieces of core directly to logging data is rarely possible because recovery is commonly poor in hard rock environments.

Six months after the reoccupation of Hole 735B during Leg 176, ODP Leg 179 returned to this location to perform sea trials of new hammer-drill casing technology. During this operation, the shipboard scientific party found time to core a site (Hole 1105A) ~1.2 km east-northeast of Hole 735B. The 158-m penetration of Hole 1105A might seem insignificant relative to the >1500 m at Hole 735B, if it were not for a coincidence discovered by the Leg 179 shipboard scientific party. Contained within the 118 m of gabbroic rock recovered from Hole 1105A is an interval roughly 60 m thick, recovered from 40 to 100 mbsf, with abundant modal Fe-Ti oxides. This observation alone is intriguing but unremarkable. However, a 60-m-thick oxide gabbro layer, buried some 210–270 mbsf, also occurs in the core recovered from Hole 735B.

The only continuous data from either Hole 735B or Hole 1105A are the files generated by downhole logging. Of particular interest to this study were FMS data. Processing FMS data results in enhancing the imaged representation of resistivity contrasts in the formation. The amount of Fe-Ti oxide (the primary conducting phase in these gabbros) varies from virtually nonexistent to 25 modal% on the scale of a few centimeters to decimeters in the oxide-bearing intervals of the lithostratigraphy. The sphere of influence of measurements for the FMS is at the same resolution (centimeters to decimeters). Excellent FMS data were recorded from the oxide-rich interval cored during Leg 179. Because the FMS logs are oriented with respect to north, this not only provides a detailed oxide-layer stratigraphy for comparison between Hole 735B and 1105A, but because these layers dip obliquely to the core axis, we can orient these features, and thus the core, with respect to north. In any event, the combination of high recovery, high-quality logging data, and the addition of a magnetic susceptibility loop to the multisensor track on board the *JOIDES Resolution* since Leg 118 allows us to more accurately resolve depths to marker horizons within each hole, reducing the error on depth calculations to nearly the resolution of the other measurements on these cores.

The objectives of this study are (1) to compare the FMS record to cores and magnetic susceptibility data from Hole 1105A to determine if specific lithologies or structural features have distinct resistivity characteristics; (2) to use the FMS data to yield orientation data on structural features in the core; and (3) depending on the success of 1 and 2, to determine if there are conspicuous groupings of reoriented structural data that can be interpreted in terms of the tectonic history of the Atlantis Bank. The ultimate goal of this research will be to develop techniques

using the high-quality logging data and high recovery from Hole 1105A to interpret and potentially correlate with the logging data from the much deeper penetration Hole 735B.

## GEOLOGIC SETTING OF HOLES 735B AND 1105A

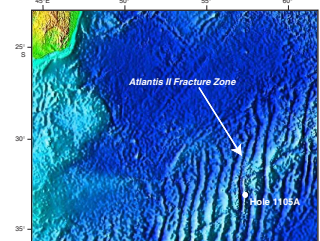
The Atlantis Bank, site of operations for ODP Legs 118, 176, and 179, is located in the rift mountains of the Southwest Indian Ridge 18 km east of the present-day axis of the Atlantis II transform fault (Fig. F1). This gabbroic massif is a 5-km-high (above the transform valley), 9-km-long, and 4-km-wide uplifted block located 93 km south of the Southwest Indian Ridge axis (Dick et al., 1991b). The top of the platform appears to be a wave-cut terrace that is now 700 meters below sea level (mbsl). The reader is referred to the “Introduction” of the “Leg 176 Summary” chapter (Shipboard Scientific Party, 1999c) and references therein for a complete documentation of our current understanding of the tectonic setting of the Atlantis Bank. In summary, the gabbroic rocks recovered during these three drilling expeditions were drilled from the center of a horst block that was originally exhumed and uplifted at an inside corner of the intersection of the Southwest Indian Ridge and the Atlantis II Fracture Zone. Whereas the geologic cross sections developed from examinations of this core record the history of deformation accompanying this exhumation, subsidence, and thermal equilibration of a huge volume of gabbro (at least 50 km<sup>3</sup>), it is imperative that we be able to orient these observations relative to the spreading axis before we can interpret them.

## PREVIOUS WORK

The FMS data recorded during Leg 179 in Hole 1105A resulted in significantly higher resolution of resistivity contrasts as compared to similar data collected during Leg 176 from Hole 735B (see “Downhole Logging” in the “Site 735B” chapter of the Leg 176 *Initial Reports* volume; Shipboard Scientific Party, 1999d). One possible explanation for the relatively poor signal (apparently saturated) from Leg 176 was the potential excessive resistivity contrast between the borehole fluid (seawater) and the resistive rocks. Leg 176 scientists suggested that if the resistivity contrast between the formation and the borehole is too large the FMS current will tend to flow into the borehole fluid rather than into the formation (Shipboard Scientific Party, 1999d). In order to alleviate this possibility, Hole 1105A was circulated with freshwater mud prior to logging.

Paleomagnetic measurements on the cores recovered from Hole 735B during Leg 118 do not include continuous magnetic susceptibility measurements (Robinson, Von Herzen, et al., 1989; Kikawa and Pariso, 1991). Only discrete samples at intervals up to several meters apart were analyzed. During Leg 179, the shipboard scientific party had the advantage of a magnetic susceptibility loop on the whole-core multisensor track and collected continuous whole-core susceptibility data. Since these data were recorded quickly and were available virtually instantaneously after measurement, they were a critical element of shipboard core description by highlighting thin intervals of abundant Fe-Ti oxide minerals. Inasmuch as the magnetic susceptibility response of a gabbro with even 1%–2% Fe-Ti oxide is significantly different than oxide-bar-

F1. Locations of the Southwest Indian Ridge, the Atlantis II Fracture Zone, and Hole 1105A, p. 14.



ren gabbro; many oxide-bearing intervals might not have been recognized without the magnetic susceptibility data on hand. Inspection of the continuous magnetic susceptibility record from the Hole 1105A cores (Fig. F2) demonstrates a low magnetic susceptibility for the upper 50 m of core, except for a thin oxide-rich layer between 37.5 and 40 mbsf. A low abundance of oxide minerals (<1 modal%) throughout the upper 50 m of Hole 1105A results in magnetic susceptibility values of less than  $2000 \times 10^{-5}$  SI. Below the low magnetic susceptibility interval is an 85-m-thick interval of oxide-rich gabbroic rocks that show markedly variable but generally high magnetic susceptibility. During Leg 179, the shipboard scientific party subdivided this interval into an upper (50–90 mbsf) and lower part (90–135 mbsf), wherein the upper had generally higher magnetic susceptibility (Pettigrew, Casey, Miller, et al., 1999).

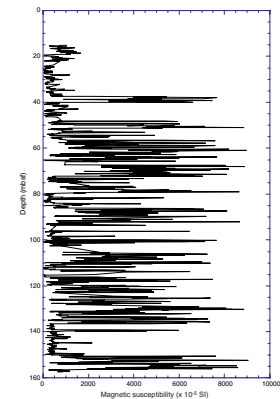
Plotting magnetic susceptibility data from discrete samples from Hole 735B cores relative to depth (Fig. F3) highlights the variable magnetic character that is reflected in the petrologic descriptions of the core (see Dick et al., 1991a). One striking feature of this plot is the interval between 200 and 300 mbsf. Above and below this interval, the data indicate variable but generally low magnetic susceptibility. At ~211 mbsf in the Hole 735B data, there is a sharp spike in the signal, which is underlain by an interval of high magnetic susceptibility ~45 m thick. In detail, this high-susceptibility interval appears to have an upper higher-susceptibility interval underlain by a lower-susceptibility interval.

In the 1500 m of rock cored in Hole 735B, the only interval with abundant magnetic oxides is in the upper 500 m and the most abundant oxides are in the interval between 180 and 260–300 mbsf, with erratically occurring oxide intervals between 400 and 500 mbsf (Shipboard Scientific Party, 1989). The similarity in thickness and character of the highest magnetic susceptibility intervals in both holes led to speculation by the Leg 179 shipboard scientific party that the oxide-rich interval recovered in both holes might represent a continuous lithostratigraphic horizon (Shipboard Scientific Party, 1999b). They suggested that by using the first high susceptibility peak in both cores as a tie point, the two records are remarkably similar, both in terms of the spacing between high magnetic susceptibility intervals and the thickness of the major oxide-rich interval. The implications of correlation between the two holes in this gabbroic massif separated by >1 km were the driving force behind initiation of this study.

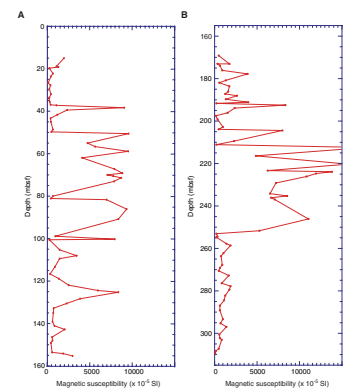
## METHODS

The objectives of this research can be summarized as successfully correlating specific lithologic and/or structural characteristics of the core with continuous logging data, particularly logging data that can be used to establish in situ core orientation. Several artifacts of recovery and ODP curation convention of hard rock cores complicated this investigation. First, whereas recovery on hard rock legs is typically low (<50%), during Leg 179 we averaged roughly 84% recovery ( $\pm 15\%$ ). These values are calculated by adding up the length of material in core liners and can be in error by several percent because pieces can be held in anomalously large or small intervals based on the random orientation of core fragments. Additionally, when the cores are curated, irregular gaps between pieces of the core are inserted where orientation along common features without missing material cannot be established with

F2. Magnetic susceptibility data, Hole 1105A, p. 15.



F3. Magnetic susceptibility data comparison, Holes 1105A and 735B, p. 16.



certainty. Thus, measurements on split or whole cores (i.e., magnetic susceptibility, core descriptions, etc.) will show discrepancies between the cumulative curated depth and the actual position in the borehole represented by the piece or measurement of interest. We can safely assume that because pieces of core longer than the diameter of the core barrel cannot exchange places during recovery that the in situ stratigraphic order of these pieces is preserved. However, with incomplete recovery, there is no record of what part of a cored interval is represented by the rock in the core barrel. Finally, the only reference point available to us is the driller's estimate of depth from the rig floor to the bit when coring commences, so all measurements are tied to this estimate.

In attempting to overcome these limitations and artifacts and because scientists commonly make observations on the millimeter to centimeter scale, scientists have historically adopted different mechanisms for accounting for the placement of specific measurements within a cored interval. The most common of these is to assume a linear expansion (and, when necessary, contraction) coefficient applied to each measurement based on the recovered length (e.g., Shipboard Scientific Party, 1999d). This method assumes that the recovered material proportionally represents the cored interval. Another method of accounting is tied to ODP curation convention (Shipboard Scientific Party, 1999a) and attaches measurements to the curated depth from the top of the cored interval. Whereas this method implies no significance to the proportion or amount of material recovered, it too is potentially in error by the difference between the cored interval and the length of core recovered.

While measuring magnetic susceptibility and describing core for this investigation, all depth measurements were made relative to the curated top of sections (see Shipboard Scientific Party, 1999d). In order to remove the artificial expansion imparted by the curation process, thus allowing nonbiased differential expansion of depth-related data sets for comparison to the continuous logging record, all depths were corrected back to our singular datum, the top of the cored interval. Cumulative errors in depth were deducted from each measurement by extracting the thickness of gaps between pieces, effectively compressing the data set to an equivalent length of the recovered core. This process can only be accomplished if the individual lengths of pieces (as measured along the center line of the piece) are known. These data are not currently recorded in the ODP database and are not routinely archived anywhere. Even more so than the driller's depth estimate that is subject to sea state and cumulative minor measurement errors, piece length remains our only accurate recovery data set for hard rocks.

Measurements of magnetic susceptibility were conducted using a Bartington model MS2 magnetic susceptibility meter, with an MS2C sensor, 80-mm dual frequency (0.47–4.70 kHz) susceptibility coil (operating frequency = 0.565 kHz), and an automated sample track. The nominal resolution is  $2 \times 10^{-6}$  SI (Blum, 1997). Susceptibility was determined at 1- and 2-cm intervals using a 1-s integration time and a 4-s period, with background measurements taken before and after the sampling sequence. For conversion to true SI volume susceptibilities, these data should be multiplied by  $10^{-5}$  and then multiplied by a correction factor to take into account the volume of material that passed through the susceptibility coils. Except for measurements near the ends of each section, this factor for a standard ODP core is  $\sim 0.7$  (Blum, 1997) and, therefore, is  $\sim 0.35$  for half cores. Values used in this paper are raw meter values, not corrected values. The data files were then edited, re-

moving values within 5 cm of the core piece ends in order to eliminate edge effects from the measurements. In cases where the cores were severely broken, this filtering required removal of the entire section from the data set. Because the raw meter scale only records values of up to 10,000 units, any values over 10,000 were recorded as anomalously low values (i.e., 10,132 would be recorded as 132), thus creating artificial variations in the data set. These artificially low values were individually removed from the data set.

Digital images were captured using a 50-mm Zeiss Distagon CF lens with f/4 aperture and floating lens element design with a medium-format camera using a Leaf digital camera back (DCB). The angle of view is 75° diagonally and 57° horizontally. Two 5000° K strobes were fired with shutter openings for each exposure. Leaf DCB/Catchlight version 3.5.3 software produces three exposed images filtered for color (red, green, and blue [RGB]) that are then spliced together to produce a 24-bit color TIFF image with the RGB color scale. Measurement and Munsell color scales were photographed next to the core for reference. Images were produced in 20-cm sections then concatenated in Adobe Photoshop to create section-length images that can be printed at various scales. Only a few image files are presented here; the complete digital image set is available from the authors.

### **Formation MicroScanner Acquisition and Processing**

The FMS is a downhole electrical imaging tool that incorporates four pads, each of which contains 16 electrodes that are in direct contact with the borehole wall, producing a vertical sampling interval of 2.5 mm. Resistance is independently measured at each electrode. The data are binned into 64 channels and translated into a graded color image illustrating resistivity contrast in the borehole wall. Light shaded areas indicate high resistivity, whereas dark shaded areas represent high conductivity. FMS images were produced after the data were processed using the GeoQuest software package GeoFrame, licensed to the Borehole Research Group of the Lamont-Doherty Earth Observatory. Files were exported from GeoFrame as GIF graphic files representing FMS data for ~50 m of borehole. Each file is roughly 1 MB. The following corrections and processing were made to the FMS data from Hole 1105A to improve data quality and interpretation:

1. Speed corrections were applied to the data to correct for the fact that measurements attributed to a cable depth are actually acquired at a somewhat different depth. This is essentially a depth correction but is also referred to as a speed correction because the depth error would not exist if the tool traveled at the same speed as the cable at the surface winch. The integration of the cable speed and the z-axis accelerometer data were used to estimate the speed and depth of the tool.
2. During operations, the FMS tool tends to stick to the borehole walls for short intervals of time (i.e., the tool remains stationary while the cable is moved for a short distance). In order to correct for this, a sticking detection threshold and recovery speed factors were applied to correct zones where the information from the cable depth and the integration of the accelerometer data are in conflict.
3. The average response of all the buttons in each pad was equalized to account for (1) the difference in gain and offset of the

preamplification circuits associated with each button; (2) differences in standoff due to pad curvature and button location with respect to the borehole wall; and (3) the difference in pressure between each pads and the borehole wall.

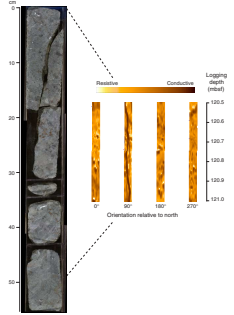
4. A faulty button detection and correction was made especially for pads that showed a significant amount of button failure. This correction interpolated the faulty button values using the values of adjacent good buttons.
5. The voltage that is applied between the button electrode and the return electrode controls the FMS button response. Because voltage saturation messages are commonly recorded in high-resistivity environments such as these, a voltage correction was applied. In this correction, the button response was divided by the EMEX (emitter exciter) voltage channel so that the response corresponds more closely to the conductivity of the formation.
6. A histogram equalization method was used as part of imaging enhancing techniques for data display. This method enhances the depiction of details in an image by optimizing the color usage (i.e., the use of colors available with equal frequency). The technique was used in two ways for highlighting different features: (1) static normalization, which is a global optimization with a window covering the entire logged interval, and (2) dynamic normalization, which is a local optimization with separate normalization computations repeated at regularly spaced positions using a 0.6-m sliding window.

## RESULTS

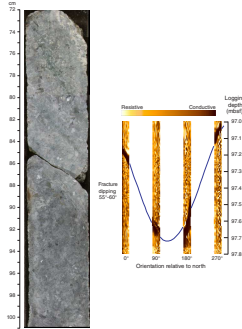
Correlation between the continuous data set (FMS) and core measurements was performed by picking specific resistivity signal intervals that could be directly related to features in the recovered core. Vertical fractures (Fig. F4) have a distinct appearance in the FMS image because the fluid in the fracture is conductive (dark color) relative to the resistive gabbro. Dipping planar fractures with high-resistivity contrasts are similarly easy to identify (Fig. F5). Areas with abundant magnetite have a distinct mottled appearance in the FMS record. Figure F6 shows a 20-cm-thick dipping oxide-rich interval. The dip on these features can be determined by fitting sinusoids using the GeoFrame software package. These data can then be related, via the fluxgate magnetometer that is part of the FMS tool string, to an azimuth, thus orienting the feature relative to magnetic north. Some 385 structural features were identified and oriented, and the resulting data are summarized in Figure F7. A bimodal distribution of dipping features is evident, with the majority of structure dipping to the south-southwest and a second mode dipping north. This is consistent with structural data recorded by FMS from Hole 735B (Iturrino et al., 2002) wherein ~25% of all picks record a dip azimuth of 180° to 240° (south-southwest) and another 25% dip from 340° to 40° (north).

Fracture networks are readily apparent in the FMS image. One example is from a core with full recovery (Core 179-1105A-13R) (Fig. F8). In the upper part of the cored interval, the gabbro is massive with a few fractures and a rare oxide-rich horizons (represented by 20-cm-thick highly conductive intervals in the FMS image). The core from this interval contains relatively long, intact pieces. The FMS image from the lower part of the cored interval shows the distinctive, almost cross-

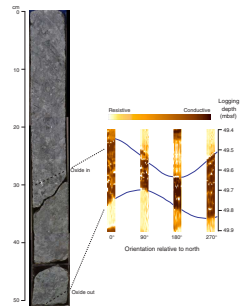
F4. A long subvertical fracture, p. 17.



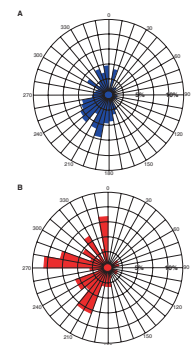
F5. Highly conductive planar features, p. 18.



F6. Dipping layer with high oxide abundance, p. 19.



F7. Dip azimuth rose diagrams, p. 20.



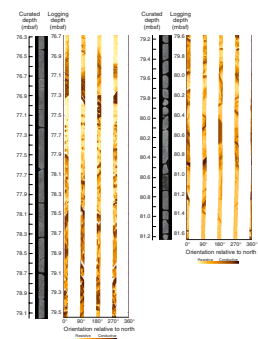
hatched pattern of a fracture network. The core recovered from this interval is broken up into smaller and more irregular length and shaped pieces. Whereas there was no recovery from the interval imaged in Figure F9, the FMS data suggest that there is a high-fracture density in this interval. Because the coring tool we use in hard rock is effectively a jackhammer, it is reasonable that these areas of high-fracture density fragment easily during drilling, resulting in poor recovery.

In addition to open fractures and oxide-bearing lithologies, intervals in the core with intense foliation presented a third distinct pattern in the FMS data that allowed for additional intervals to be correlated with confidence. Figure F10 shows the strong foliation apparent in an interval of core, and the corresponding FMS image. Less spectacular but just as useful in terms of correlation, intervals with very coarse to pegmatitic grain size have a patchy FMS signal, which is also illustrated in Figure F10. Our ability to match up many of these features in a short core intervals on a one-to-one basis (Fig. F11) enhanced the confidence in the picks made on specific intervals.

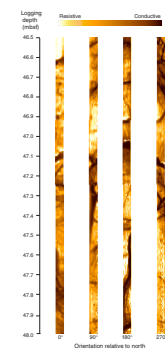
Based core observations, the magnetic susceptibility data, and FMS records we were able to compile more than 70 high-confidence oxide correlation intervals (Table T1). Several observations that are locally and universally applicable to ODP hard rock data handling result from this investigation. First, most of the oxide-bearing intervals dip to the south-southwest (42%; average dip = 38°) (see Fig. F6) with a smaller mode dipping north (10%; average dip = 40°). This is coincident with the major structural feature orientations identified from Hole 735B (Iturrino et al., 2002) and the majority of structural features recognized from Site 1105. There is, however, a subset of oxide-bearing intervals (~20%) that strike north to south with a shallower average dip (25°) to the west, toward the present transform axis. Nearly all of the west-dipping oxide-bearing intervals are thin (<20 cm thick) oxide-rich layers, whereas the majority of the north- and south-dipping intervals are thicker intervals (≥1 m) and oxide is more disseminated. Paleomagnetic data from Leg 176 (Shipboard Scientific Party, 1999d) suggest that the uplifted block of the Atlantis Bank has seen ~80° of clockwise rotation since formation. If we interpret the disseminated oxide gabbros as magmatic and note that the orientations of these features are consistent with the structural features (predominantly fractures) measured from both Hole 735B and Hole 1105A, then it is possible that all these features were introduced in the same stress field. Applying an 80° counterclockwise rotation to these data (to restore them to their orientation when the paleomagnetic declination was set) reveals that the principal stress direction on this gabbro body at the time of formation was parallel to the ridge axis (since the corrected strike of all these features would be approximately north–south).

Second, and more generally, of the 30 cores recovered, the compressed magnetic susceptibility record of 23 cores correlated directly with the continuous FMS record; no expansion or contraction of the data was necessary to establish correlations (see Fig. F12). Four cores did not have sufficient tie points to make any assessment of whether or not they represented continuous recovery. Only three cores required even partial expansion between high-confidence intervals to produce a reasonable correlation between magnetic susceptibility and FMS data. This indicates, at least for the core recovered from Hole 1105A and likely for most hard rock drilling, that the recovered core is more than likely the first material to enter the core barrel. After a certain amount of material has been captured, because of either mechanical fracturing or rotational

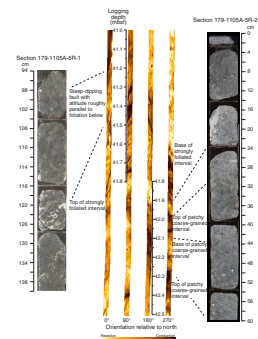
F8. Core and FMS images from Core 179-1105A-13R, p. 21.



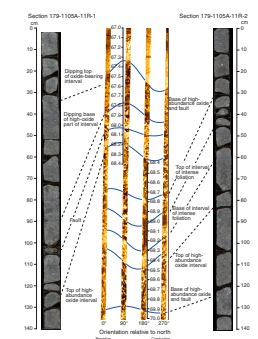
F9. FMS interval showing a pattern of intense fracture, p. 22.



F10. Coarse-grained to pegmatitic intervals, p. 23.



F11. High confidence level of correlative intervals based on multiple tie points, p. 24.



abrasion, no more core enters the core barrel. This is supported by anecdotal observations from many hard rock legs where core recovery typically improves when we reduce the length of the cored interval. Our hard rock coring tools recover a limited amount of material, regardless of the length of the cored interval. This suggests that in instances where recovery takes precedence over time in a hole and the hole is stable, it may be prudent to reduce coring intervals, possibly to as little as 2 m to enhance recovery. It also demonstrates that coring tools used in hard rock do not sample downhole lithologic sequences proportionally. In addition to evidence that we do not have high recovery in intervals that are intensely fractured (regardless of lithology), the data from Hole 1105A indicate that we routinely recover only the upper part of each cored interval. Attempts to interpret downhole lithologic variations based on linear expansion of the recovered core should be viewed with skepticism. Differences of up to a few tens of centimeters are evident between the estimate of depth to the top of a cored interval and the correlation of index features in that interval with the FMS log (Table T2). Although there has been some speculation on the possibility of a pedestal of material being left at the bottom of the borehole between coring intervals, minor errors in the estimate of the depth to the top and/or bottom of the cored interval are the most likely controls on intervals of anomalously high recovery in hard rock (in excess of 100%). The possibility of these errors being cumulative is the most likely explanation for the discrepancy between the depth to the bottom of Hole 735B when it was left in 1987 (500.5 mbsf) and reoccupied in 1997 (504.5 mbsf) despite the exact same depth to the collar of the hole.

## SUMMARY

The combination of FMS logging data and high recovery with detailed lithologic descriptions and whole and split core magnetic susceptibility measurements yields new and unique insights into the coring and recovery process in hard rocks. This study also has direct application to characterizing structural information that is usually challenging in subseafloor hard rock coring. Finally, the results from this investigation provide specific recommendations on future (and past) coring, logging, and data handling in hard rock environments. These points can be summarized as follows:

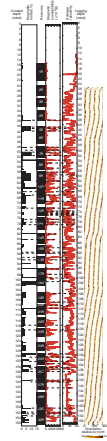
1. FMS data yield images illustrating resistivity contrasts that can be used to distinguish between fractures, foliation, and oxide-bearing lithologies in the gabbros from Hole 1105A.
2. The FMS data provide support for the anecdotal observations that our current hard rock coring tools do not perform particularly well when attempting to recover core from highly fractured formations.
3. The cores from Hole 1105A demonstrate, in most cases, that linear expansion of data from the recovered core to interpret intervals of low recovery is not an accurate methodology. Inasmuch as in most cases the core recovered is the first material to enter the core barrel (as opposed to piecemeal or random recovery) and recovery seems to stop when the barrel becomes obstructed, the ODP convention of shunting all the core pieces to the top of the cored interval for curation is, at least in cases of moderate to high recovery, a reasonable practice.

---

**T1.** Orientation estimates for oxide-bearing lithologies, p. 27.

---

**F12.** Downhole compilation of magnetite-bearing lithologies, filtered magnetic susceptibility, average FMS data, and FMS image, p. 25.



---

**T2.** Curated depth vs. logging depth, p. 29.

---

4. Most critically, the high core recovery and high confidence with which we can orient individual features in the core allows us to orient structural features within the geomagnetic reference frame with high confidence. By reorienting structural features according to paleomagnetic measurements, we infer that the direction of principle stress during the early crystallization and deformation history of the gabbroic magma now exposed on the Atlantis Bank was parallel to the Southwest Indian Ridge axis.

## **ACKNOWLEDGMENTS**

This research used samples and/or data provided by the Ocean Drilling Program (ODP). ODP is sponsored by the U.S. National Science Foundation (NSF) and participating countries under management of Joint Oceanographic Institutions (JOI), Inc. Funding for this research was provided by a United States Science Support Panel postcruise research grant to DJM. This manuscript benefitted from thorough and insightful reviews by Jack Casey, Bernard C  lerier, Tim Brewer, and an anonymous reviewer.

## REFERENCES

- Blum, P., 1997. Physical properties handbook: a guide to the shipboard measurement of physical properties of deep-sea cores. *ODP Tech. Note*, 26 [Online]. Available from World Wide Web: <<http://www-odp.tamu.edu/publications/tnotes/tn26/INDEX.HTM>>. [Cited 2002-08-15]
- Cannat, M., and Pariso, J., 1991. Partial reorientation of the deformational structures at Site 735 using paleodeclination measurements. In Von Herzen, R.P., Robinson, P.T., et al., *Proc. ODP, Sci. Results*, 118: College Station, TX (Ocean Drilling Program), 409–414.
- Célérier, B., MacLeod, C.J., and Harvey, P.K., 1996. Constraints on the geometry and fracturing of Hole 894G, Hess Deep, from Formation MicroScanner logging data. In Mével, C., Gillis, K.M., Allan, J.F., and Meyer, P.S. (Eds.), *Proc. ODP, Sci. Results*, 147: College Station, TX (Ocean Drilling Program), 329–345.
- Dick, H.J.B., Meyer, P.S., Bloomer, S., Kirby, S., Stakes, D., and Mawer, C., 1991a. Lithostratigraphic evolution of an in-situ section of oceanic Layer 3. In Von Herzen, R.P., Robinson, P.T., et al., *Proc. ODP, Sci. Results*, 118: College Station, TX (Ocean Drilling Program), 439–538.
- Dick, H.J.B., Natland, J.H., Alt, J.C., Bach, W., Bideau, D., Gee, J.S., Haggas, S., Hertogen, J.G.H., Hirth, G., Holm, P.M., Ildefonse, B., Iturrino, G.J., John, B.E., Kelley, D.S., Kikawa, E., Kingdon, A., LeRoux, P.J., Maeda, J., Meyer, P.S., Miller, D.J., Naslund, H.R., Niu, Y., Robinson, P.T., Snow, J., Stephen, R.A., Trimby, P.W., Worm, H.-U., and Yoshinobu, A., 2000. A long in situ section of the lower ocean crust: results of ODP Leg 176 drilling at the Southwest Indian Ridge. *Earth Planet. Sci. Lett.*, 179:31–51.
- Dick, H.J.B., Schouten, H., Meyer, P.S., Gallo, D.G., Bergh, H., Tyce, R., Patriat, P., Johnson, K.T.M., Snow, J., and Fisher, A., 1991b. Tectonic evolution of the Atlantis II Fracture Zone. In Von Herzen, R.P., Robinson, P.T., et al., *Proc. ODP, Sci. Results*, 118: College Station, TX (Ocean Drilling Program), 359–398.
- Iturrino, G.J., Ildefonse, B., and Boitnott, G., 2002. Velocity structure of the lower oceanic crust: results from Hole 735B, Atlantis II Fracture Zone. In Natland, J.H., Dick, H.J.B., Miller, D.J., and Von Herzen, R.P. (Eds.), *Proc. ODP, Sci. Results*, 176 [Online]. Available from World Wide Web: <[http://www-odp.tamu.edu/publications/176\\_SR/chap\\_05/chap\\_05.htm](http://www-odp.tamu.edu/publications/176_SR/chap_05/chap_05.htm)>. [Cited 2002-08-15]
- Kikawa, E., and Pariso, J.E., 1991. Magnetic properties of gabbros from Hole 735B, Southwest Indian Ridge. In Von Herzen, R.P., Robinson, P.T., et al., *Proc. ODP, Sci. Results*, 118: College Station, TX (Ocean Drilling Program), 285–307.
- National Geophysical Data Center, 2003. *Satellite and Information Services* [Online]. Available from World Wide Web: <<http://www.ngdc.noaa.gov/mgg/image/2minsurface/00N045E.html>>. [Cited 2003-01-20]
- Pettigrew, T.L., Casey, J.F., Miller, D.J., et al., 1999. *Proc. ODP, Init. Repts.*, 179 [Online]. Available from World Wide Web: <[http://www-odp.tamu.edu/publications/179\\_IR/179TOC.HTM](http://www-odp.tamu.edu/publications/179_IR/179TOC.HTM)>. [Cited 2003-01-20]
- Robinson, P.T., Von Herzen, R., et al., 1989. *Proc. ODP, Init. Repts.*, 118: College Station, TX (Ocean Drilling Program).
- Shipboard Scientific Party, 1989. Site 735. In Robinson, P.T., Von Herzen, R., et al., *Proc. ODP, Init. Repts.*, 118: College Station, TX (Ocean Drilling Program), 89–222.
- , 1993. Site 894. In Gillis, K., Mével, C., Allan, J., et al., *Proc. ODP, Init. Repts.*, 147: College Station, TX (Ocean Drilling Program), 45–108.
- , 1999a. Explanatory notes. In Pettigrew, T.L., Casey, J.F., Miller, D.J., et al., *Proc. ODP, Init. Repts.*, 179 [Online]. Available from World Wide Web: <[http://www-odp.tamu.edu/publications/179\\_IR/chap\\_03/chap\\_03.htm](http://www-odp.tamu.edu/publications/179_IR/chap_03/chap_03.htm)>. [Cited 2003-01-20]
- , 1999b. Hammer Drill Site (1104 and 1106) and Site 1105. In Pettigrew, T.L., Casey, J.F., Miller, D.J., et al., *Proc. ODP, Init. Repts.*, 179, 1–183 [Online]. Available

from World Wide Web: <[http://www-odp.tamu.edu/publications/179\\_IR/VOLUME/CHAPTERS/CHAP\\_04.PDF](http://www-odp.tamu.edu/publications/179_IR/VOLUME/CHAPTERS/CHAP_04.PDF)>. [Cited 2003-01-20]

———, 1999c. Leg 176 summary. *In* Dick, H.J.B., Natland, J.H., Miller, D.J., et al., *Proc. ODP, Init. Repts.*, 176, 1–70 [Online]. Available from World Wide Web: <[http://www-odp.tamu.edu/publications/176\\_IR/VOLUME/CHAPTERS/CHAP\\_01.PDF](http://www-odp.tamu.edu/publications/176_IR/VOLUME/CHAPTERS/CHAP_01.PDF)>. [Cited 2003-01-20]

———, 1999d. Site 735. *In* Dick, H.J.B., Natland, J.H., Miller, D.J., et al., *Proc. ODP, Init. Repts.*, 176, 1–314 [Online]. Available from World Wide Web: <[http://www-odp.tamu.edu/publications/176\\_IR/VOLUME/CHAPTERS/CHAP\\_03.PDF](http://www-odp.tamu.edu/publications/176_IR/VOLUME/CHAPTERS/CHAP_03.PDF)>. [Cited 2003-01-20]

**Figure F1.** Satellite altimetry map showing a portion of the Southwest Indian Ridge, the Atlantis II Fracture Zone, and the location of Hole 1105A. The base image is from National Geophysical Data Center (2003).

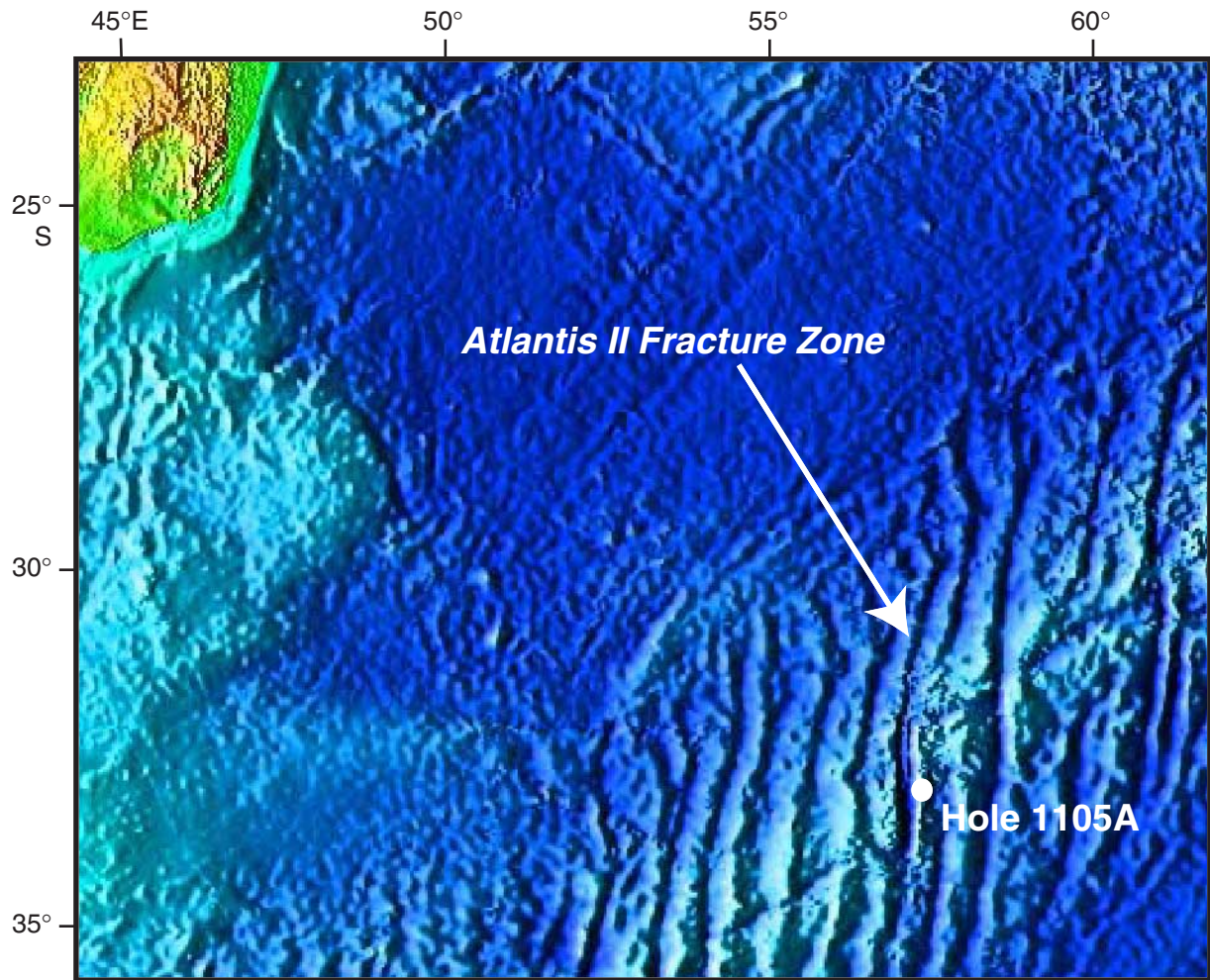
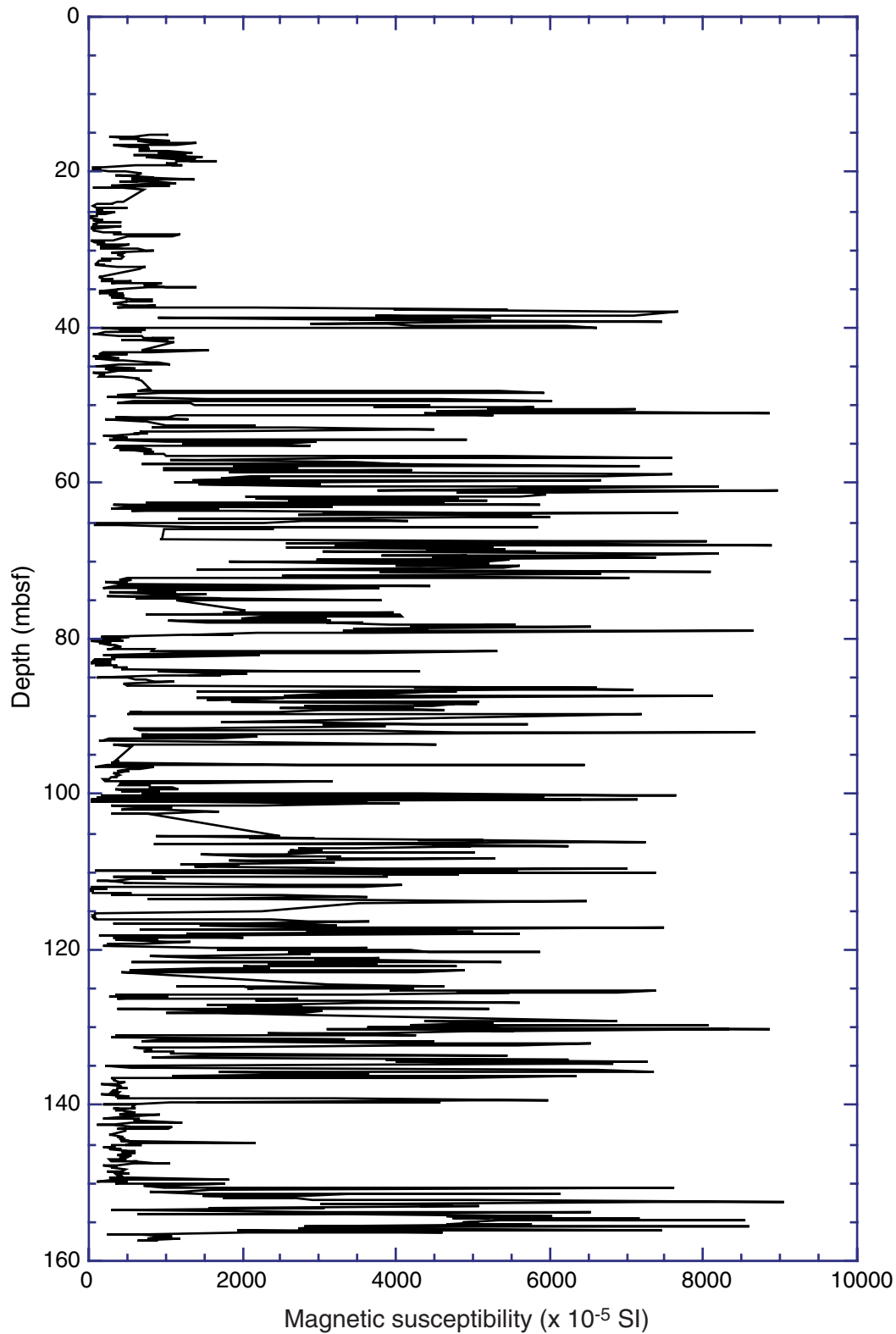
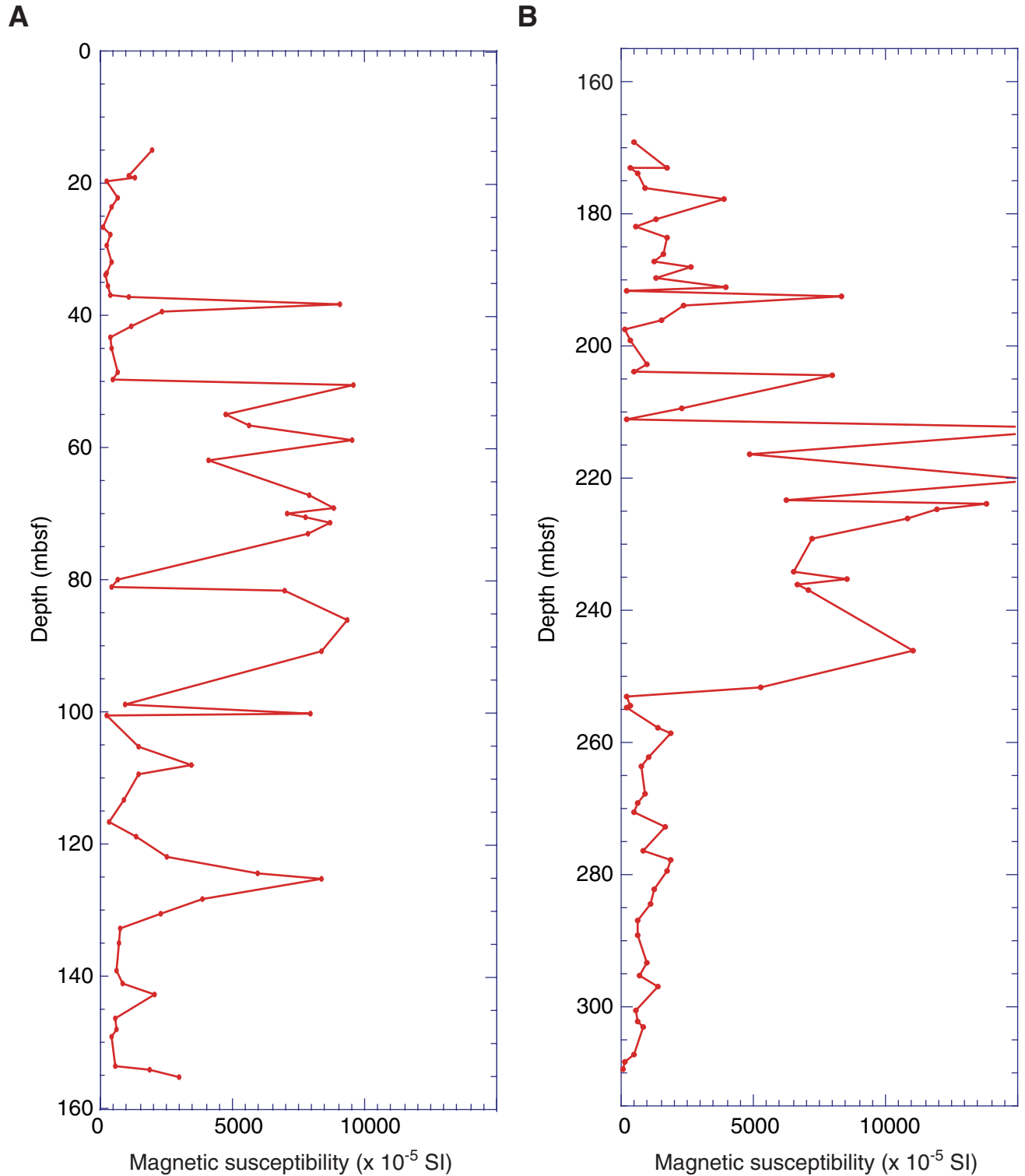


Figure F2. Continuous whole-core magnetic susceptibility data from Hole 1105A. High-susceptibility layers are oxide-rich gabbro; low-susceptibility intervals are gabbro and olivine gabbro. Figure modified from Shipboard Scientific Party (1999b). Note that the units in the original figure were reported as SI and are corrected here to  $\times 10^{-5}$  SI.



**Figure F3.** Comparison of magnetic susceptibility data from cores from (A) Hole 1105A and (B) Hole 735B. Hole 1105A data (from the whole-core multisensor track) have been filtered to remove piece end effects (all measurements within 5 cm of the end of a core piece have been deleted). Hole 735B data (discrete mini-cores) have been registered such that the first high-susceptibility peak coincides with the first high-susceptibility peak in Hole 1105A data. Hole 1105A data were selected to most closely approximate the relative depths of Hole 735B discrete samples, based on the single correlative point (38.4 mbsf in Hole 1105A data and 212.5 mbsf in Hole 735B data).



**Figure F4.** A long subvertical fracture that is superbly imaged in FMS data (interval 179-1105A-23R-2, 0–50 cm). All FMS images presented here are from dynamically processed files. This and all subsequent core images are high-resolution JPEG files. In electronic format, these can be enlarged at least 800% (to examine details) before pixelation distorts the image.

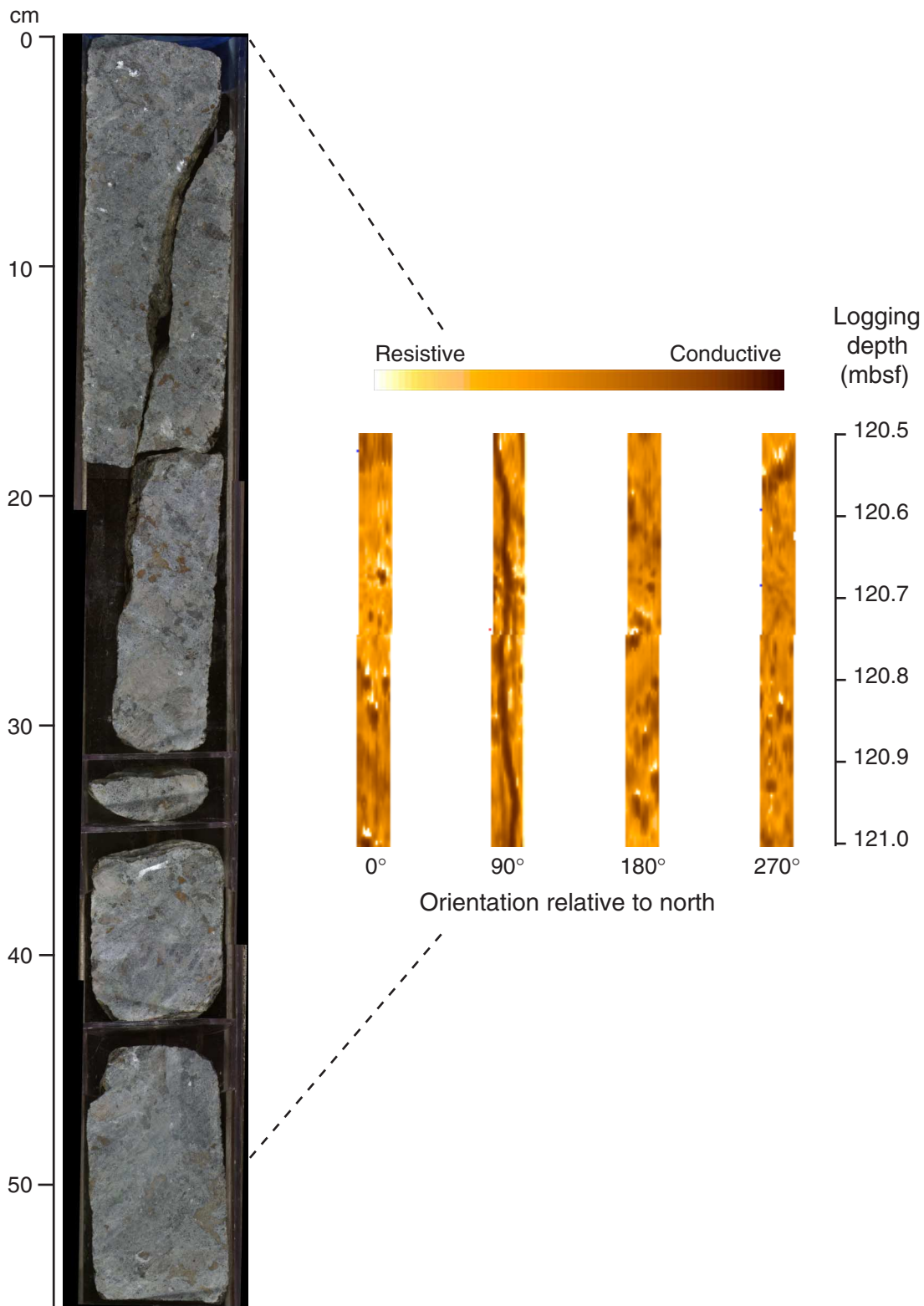
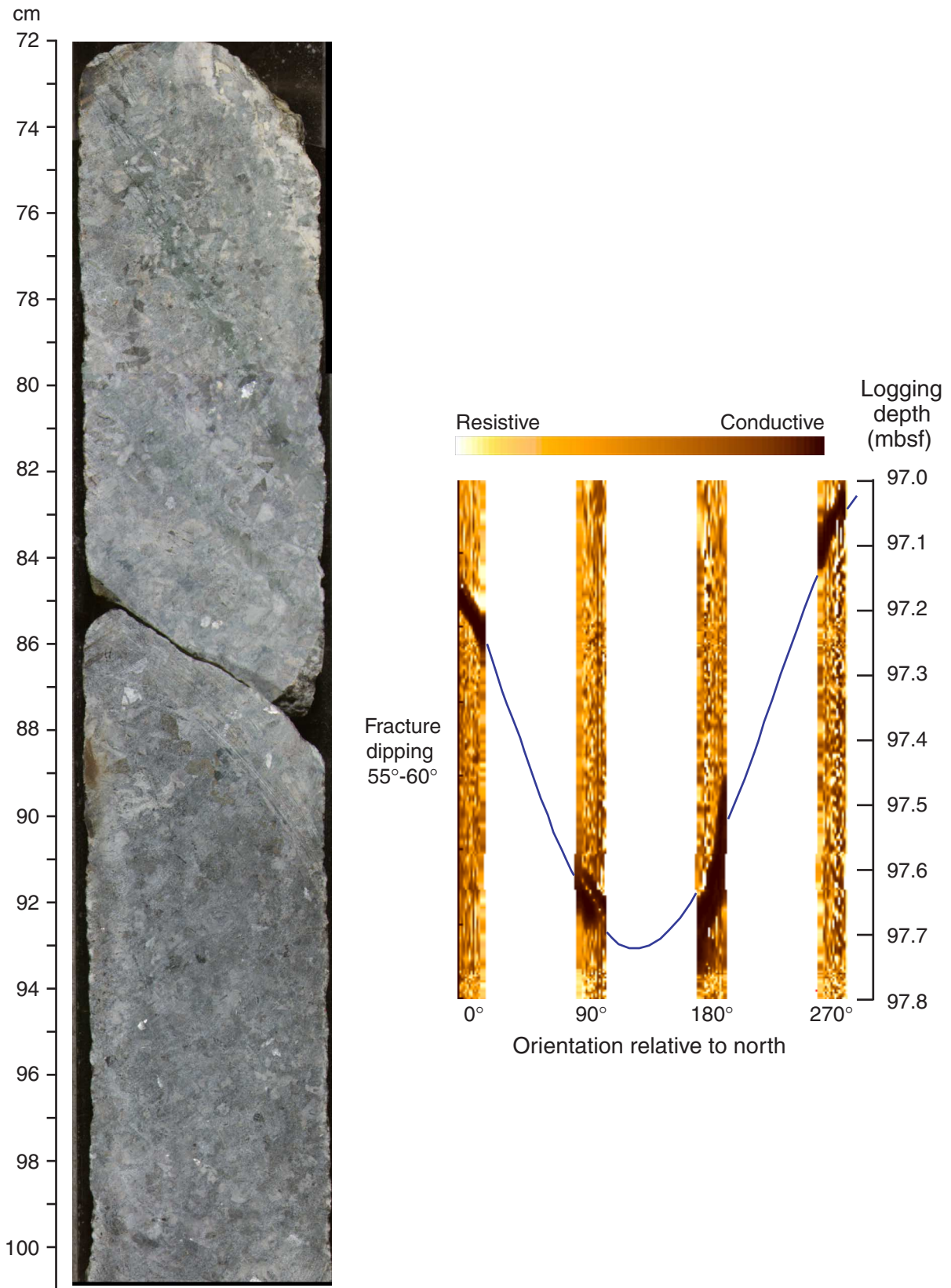


Figure F5. Planar fractures are highly conductive (dark) relative to surrounding resistive gabbro (Section 179-1105A-17R-1). A sinusoid matched to these conductive intervals defines a unique orientation. This fracture measured in the core dips 58°; the independently picked sinusoid (blue lines in all FMS images) indicates a dip of 60°.



**Figure F6.** Dipping layer with high oxide abundance (>10%) (interval 179-1105A-7R-1, 0–50 cm). The mottled pattern in the FMS image is characteristic of high oxide abundance in these cores, probably a result of disseminated oxide grains (conductive) in a resistive gabbroic host. The preserved thickness of this interval is virtually identical to the thickness imaged in the log, indicating that despite the break in recovery, effectively no material was lost.

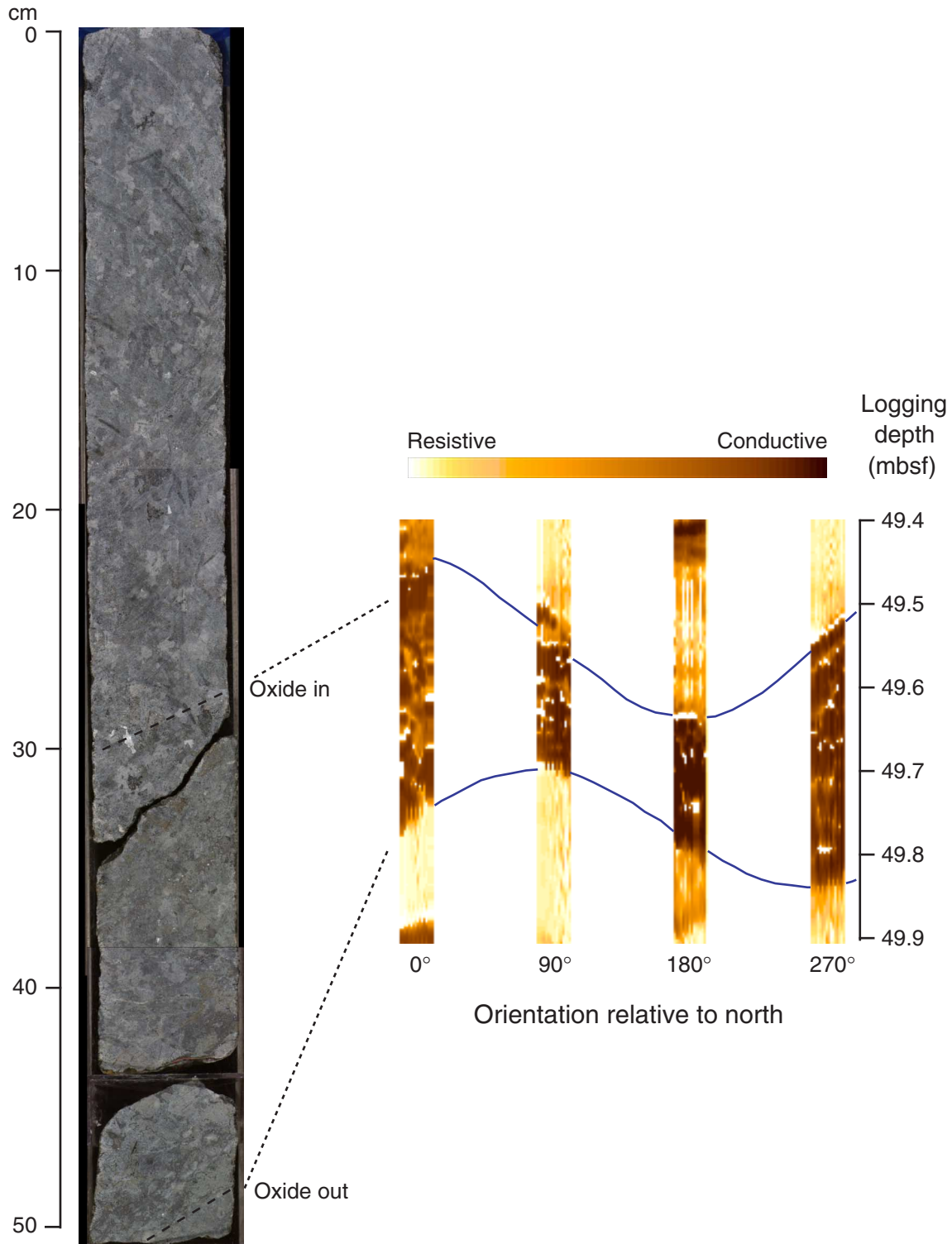
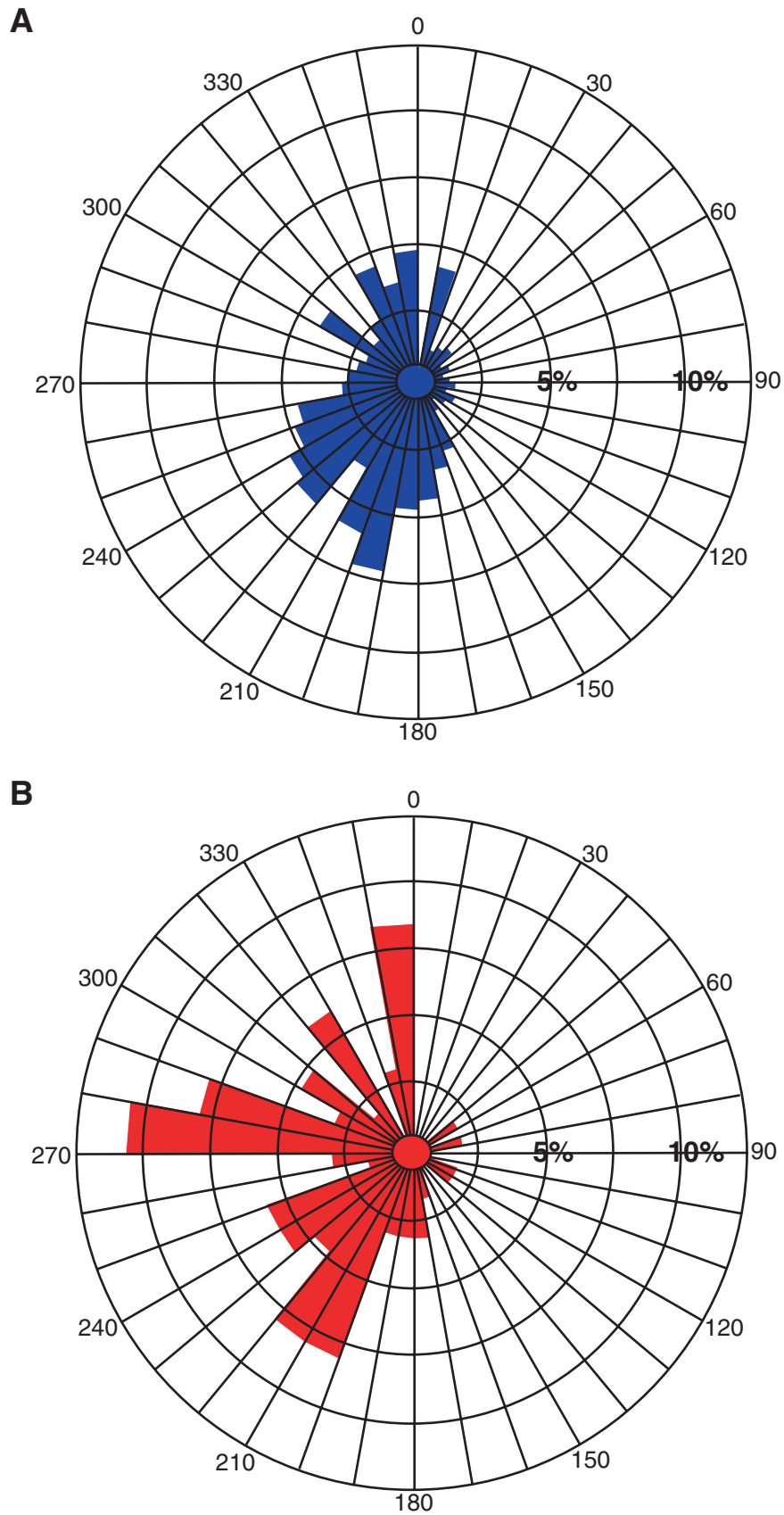


Figure F7. Dip azimuth rose diagrams for (A) 385 structural features (fractures, layers, etc.) determined using GeoFrame analysis of FMS data and (B) the subset of 71 oxide-bearing intervals.



**Figure F8.** Core and FMS images from Core 179-1105A-13R. Reduced core piece length and increased piece shape irregularity are coincident with an increase in FMS image patterns interpreted to represent fractures in the lower part of the interval.

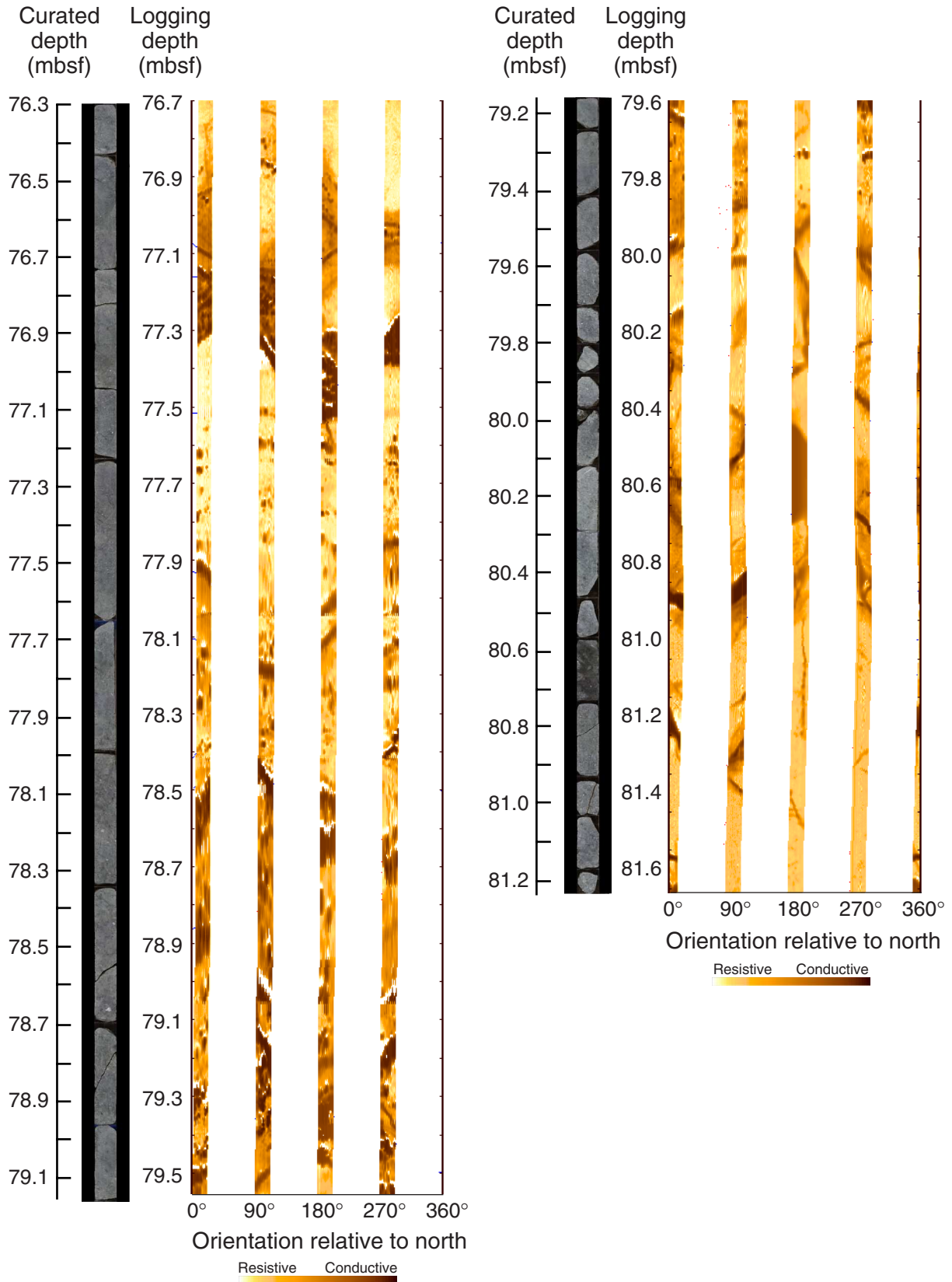


Figure F9. FMS interval from 46.5 to 48 mbsf (equivalent to the lower part of the interval represented by Core 179-1105A-6R) showing a pattern of intense fracture that probably induced low recovery.

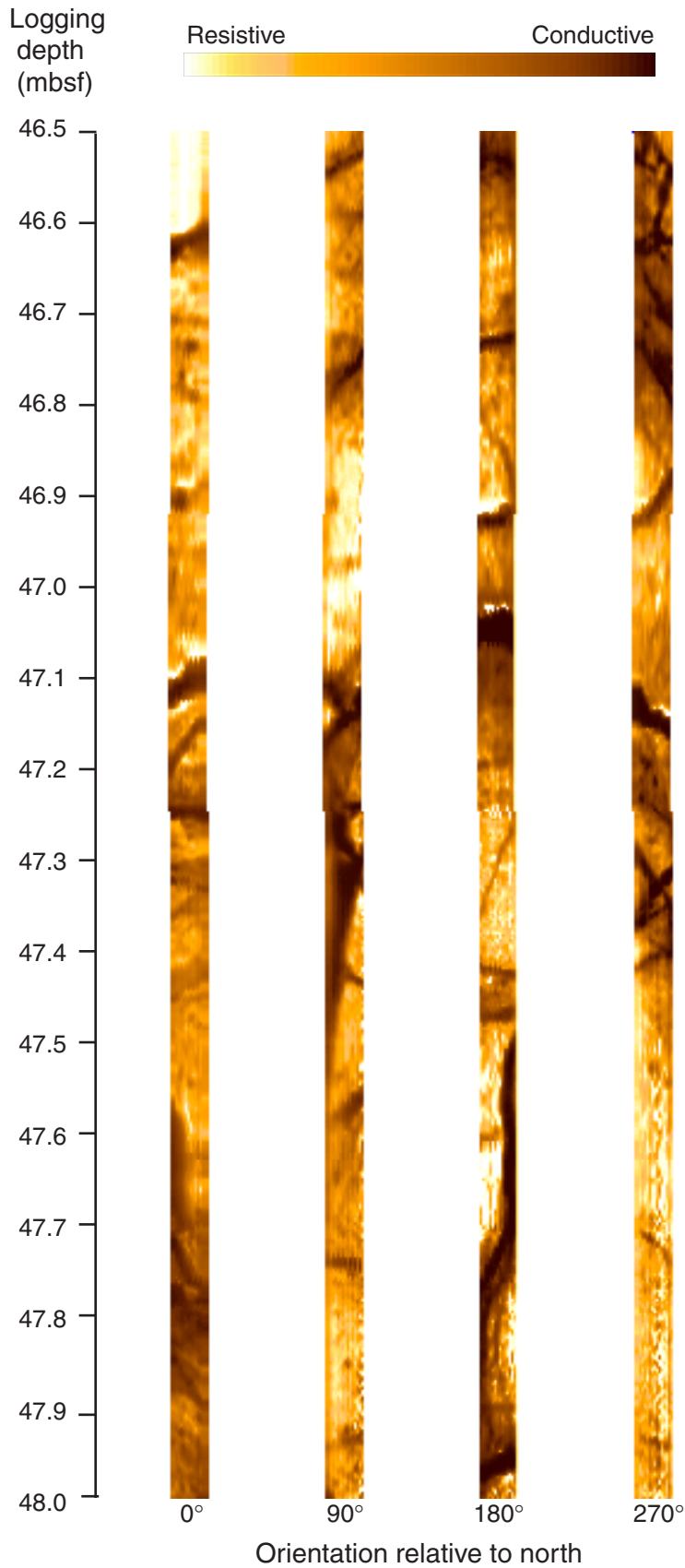
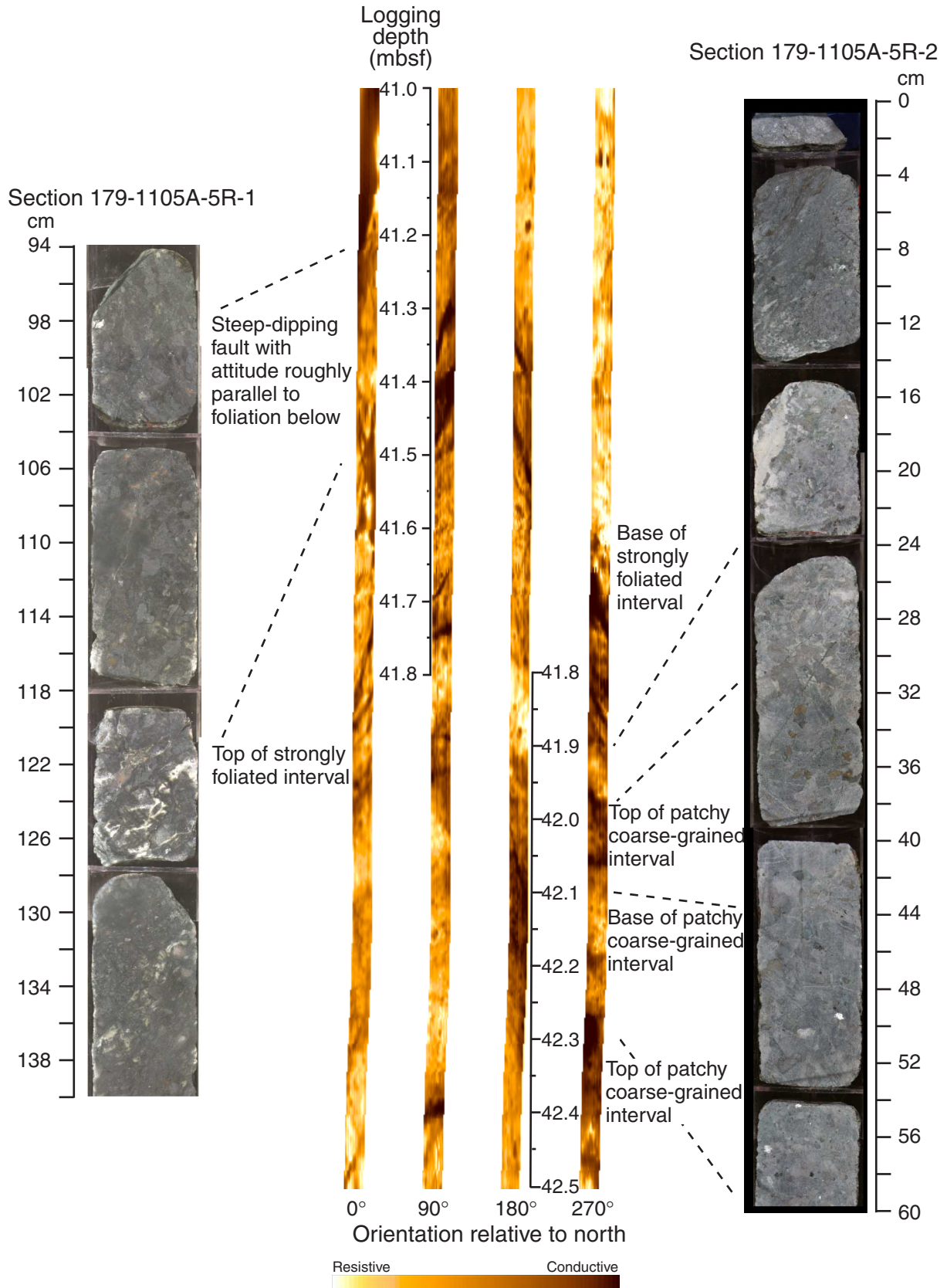
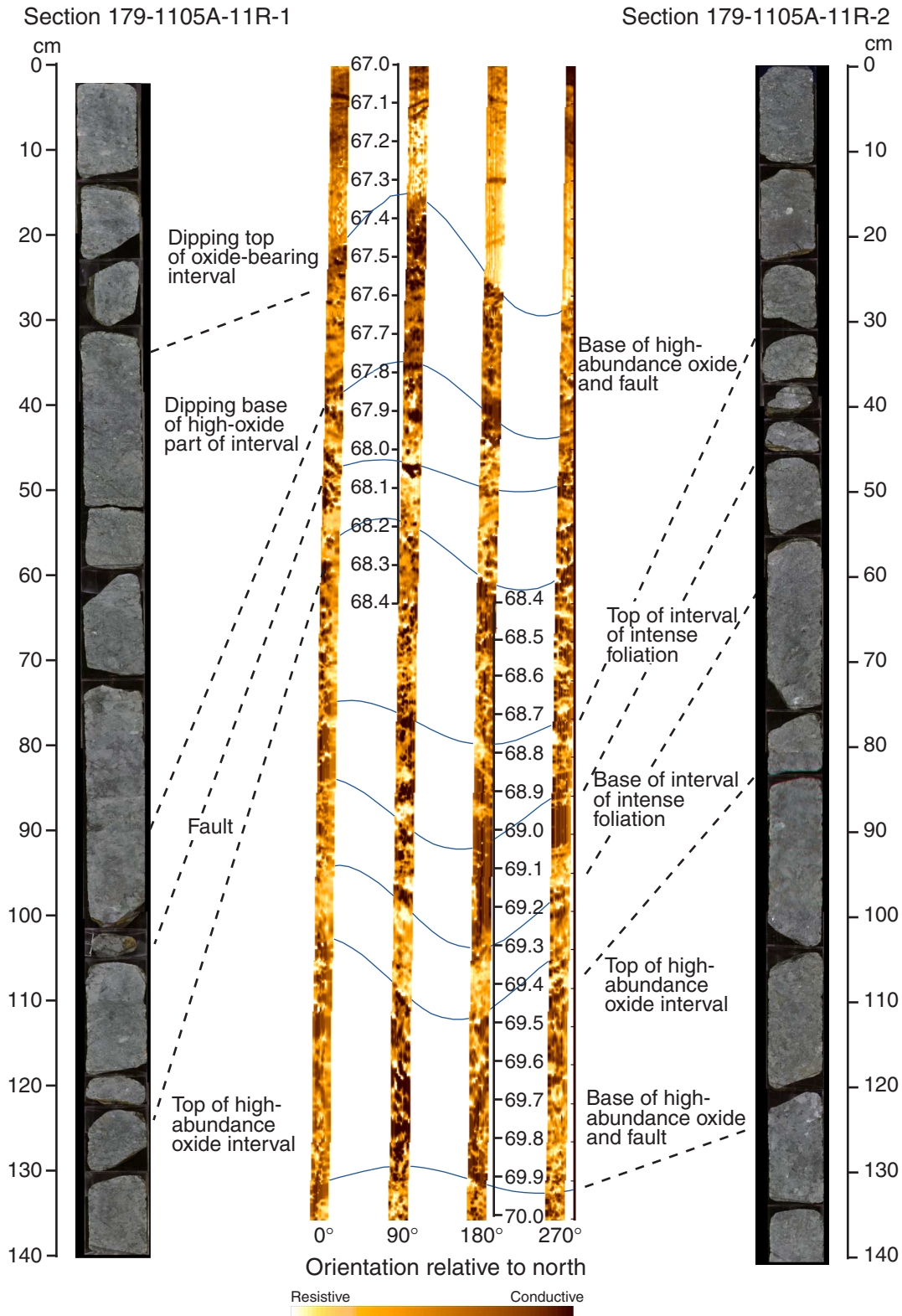


Figure F10. Foliation imparts a distinct pattern to the FMS image as represented by the interval between 41 and 42.5 mbsf (logging depth). Coarse-grained to pegmatitic intervals have a patchy appearance because of conductivity differences between large mineral grains.



**Figure F11.** The high confidence level of correlative intervals is based on multiple tie points involving different features occurring within the same section or consecutive sections of core. Nine tie points are apparent in Sections 1 and 2 of Core 179-1105A-11R, and despite the many breaks in the core, the relative distance between these points remains virtually the same as their separation in the continuous FMS image, again suggesting very little loss of material.



**Figure F12.** Downhole compilation of magnetite-bearing lithologies (left panel), filtered (removing piece end effects) magnetic susceptibility (left center panel), average FMS data (right center panel), and FMS image (right panel). The first column shows the abundance of magnetite downhole relative to depth and hung from the driller's depth estimate. Included alongside this column is a graphic representation of the amount of recovery per core (black shade) relative to cored intervals (gaps between black rectangles). The second column shows split-core magnetic susceptibility data. The third column shows the binned electric resistivity data (min = 0, max = 64) from the average of four receivers on pad 1 of the FMS. The fourth column shows a color-coded illustration of FMS data for all four pads. All of these data have been plotted at the same depth scale. Major correlative tie points are noted as dashed lines. (This figure is also available in an **oversized format. Figure shown on next page.**)

Figure F12 (continued). (Caption shown on previous page.)

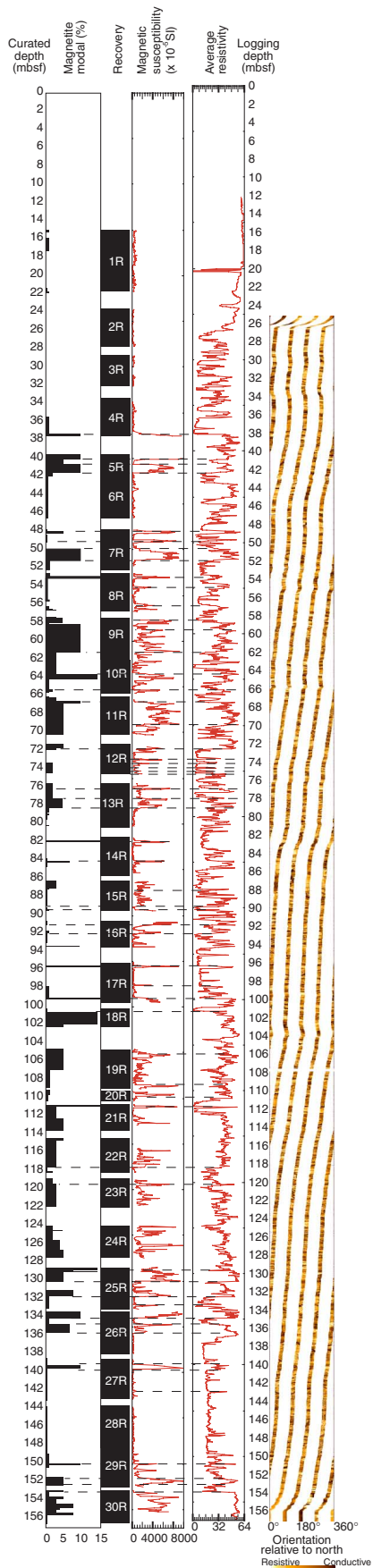


Table T1. Orientation estimates for oxide-bearing lithologies, Hole 1105A. (See table note. Continued on next page.)

Core, section	Piece	Oriented	Top (cm)	Depth (mbsf)		Feature type	Dip (°)	Dip azimuth (°)
				Curated	Logging			
179-1105A-								
3R-2	12	Y	120	31.10	31.60	Steep-dipping oxide veins	60	255
4R-4	4	Y	25	37.70	38.30	Top of dipping oxide layer	45	230
5R-1	8	Y	120	39.50	39.90	Oxide-gabbro/gneissic oxide gabbro	45	120
5R-1	2	Y	36	38.70	39.10	Base crystal-plastic foliation and oxide out	25	161
7R-1	1	Y	40	48.20	48.70	Top of oxide gabbro	45	200
7R-1	5	Y	70	48.50	49.00	Base of oxide gabbro	45	205
7R-1	10	Y	135	49.15	49.60	Top of gneissic oxide gabbro	25	180
7R-2	2	Y	25	49.40	49.80	Base of gneissic oxide gabbro	55	200
7R-2	5	Y	80	49.90	50.10	Increase in oxide abundance	45	205
7R-3	3	Y	1	51.40	51.90	Base of gneissic oxide gabbro	70	170
8R-2	4	Y	47	53.90	54.50	Top of oxide gabbro	30	265
8R-2	8	Y	133	54.10	54.70	Base of oxide gabbro	30	285
8R-3	1	Y	20	55.00	55.60	Base of disseminated oxide gabbro	15	330
8R-3	10	Y	125	56.10	56.50	Top of oxide gabbro	20	310
9R-1	2	Y	34	58.20	58.70	Top of oxide gabbro	30	210
9R-3	6	Y	76	61.20	61.70	Base of oxide gabbro	30	230
10R-1	2	Y	20	62.20	62.90	Top of oxide gabbro	30	200
10R-1	3	Y	40	62.40	63.20	Base of oxide gabbro	25	240
10R-1	3	Y	70	62.70	63.30	Top of oxide gabbro	35	250
10R-1	3	Y	80	62.80	63.40	Base of oxide gabbro	35	270
10R-2	4	Y	30	63.80	64.40	Top oxide gabbro	40	320
10R-2	8	Y	90	65.00	65.70	Base oxide gabbro	45	350
11R-1	5	Y	45	67.40	67.80	Top of oxide gabbro	50	345
11R-3	2	Y	35	69.90	70.20	Decrease in oxide abundance	55	355
12R-1	12	N	88	72.20	72.60	Base of oxide gabbro	40	110
13R-1	2	Y	26	76.50	76.80	Top of oxide layer	25	305
13R-1	2	Y	35	76.60	76.90	Base of oxide layer	25	295
13R-1	3C	Y	66	77.00	77.20	Top of oxide layer	40	225
13R-1	3D	Y	85	77.20	77.40	Base of oxide layer	35	230
13R-2	2	Y	50	78.10	78.50	Top of oxide layer	25	290
13R-2	2	Y	60	78.20	78.60	Base of oxide layer	30	280
13R-2	4	Y	125	78.80	79.20	Top of oxide layer	25	290
13R-3	3	Y	25	79.20	79.60	Base of oxide layer	35	320
16R-1	13	Y	60	91.20	91.90	Bottom of strong foliation	65	220
16R-1	4	Y	30	90.90	91.60	Top of strong foliation	10	270
16R-2	2	Y	10	92.00	92.50	Steep-dipping oxide layer	10	270
17R-1	3	Y	47	96.10	96.40	Top of dipping oxide gabbro	25	200
17R-1	6	Y	70	96.30	96.50	Base of dipping oxide gabbro	25	210
17R-3	18	Y	147	99.70	100.00	Top of foliated oxide layer	25	270
17R-4	4	Y	50	100.30	100.60	Base of foliated oxide gabbro	25	270
18R-1	11	Y	117	101.30	102.30	Base of foliated oxide gabbro	45	300
18R-1	4	Y	35	100.50	101.50	Top of oxide gabbro	45	300
19R-1	5	Y	50	105.70	106.10	Top of oxide gabbro	25	10
19R-1	6	Y	120	106.30	106.70	Top of oxide gabbro	25	270
19R-1	6	Y	110	106.10	106.50	Base of oxide gabbro	25	290
19R-3	2	Y	20	108.10	108.40	Base of oxide gabbro	25	300
19R-4	1	Y	1	109.20	109.50	Top of oxide gabbro	25	320
21R-1	8A	Y	90	111.70	111.90	Oxide gabbro	25	30
22R-2	4	Y	66	117.10	117.20	Base of foliated oxide gabbro	30	75
22R-3	4	Y	70	118.30	118.40	Base of oxide gabbro	30	355
23R-1	7	Y	70	120.10	120.10	Top of oxide gabbro	30	240
23R-1	8	Y	90	120.30	120.30	Base of oxide gabbro	30	240
24R-1	6	Y	150	125.30	125.70	Foliated oxide gabbro	20	170
24R-2	7	Y	53	126.20	126.60	Crosscutting fracture	30	260
24R-3	4	Y	45	127.20	127.40	Base of oxide gabbro	55	350
25R-1	1	Y	7	129.10	129.30	Top of strongly foliated oxide gabbro	25	55
25R-2	1	Y	20	130.60	130.80	Base of strongly foliated oxide gabbro	35	190
25R-2	4	Y	132	131.70	131.90	Top of foliated oxide gabbro	30	200
25R-3	6	Y	57	132.30	132.50	Base of foliated oxide gabbro	20	230
26R-1	2	Y	75	134.70	134.90	Base of oxide gabbro	35	320
26R-2	1	Y	2	135.30	135.40	Top of oxide gabbro	50	320
26R-2	1	Y	20	135.50	135.60	Base of oxide gabbro	15	355
27R-1	1	Y	47	139.10	139.80	Top of oxide gabbro	20	50
27R-1	3	Y	95	139.70	140.50	Base of oxide gabbro	20	50
28R-1	3	Y	104	144.70	144.70	Top of oxide gabbro	15	225
28R-2	1	Y	4	144.80	144.80	Base of oxide gabbro	30	270

**Table T1 (continued).**

Core, section	Piece	Oriented	Top (cm)	Depth (mbsf)		Feature type	Dip (°)	Dip azimuth (°)
				Curated	Logging			
28R-3	2	Y	140	147.00	147.00	Subhorizontal fracture	30	270
29R-1	4	Y	100	149.40	149.80	Top of foliated oxide gabbro	20	170
29R-2	3	Y	94	150.60	151.10	Oxide gabbro pod	45	210
29R-3	4	Y	40	151.30	151.70	Top of strongly foliated oxide gabbro	45	210
29R-4	2	Y	40	152.70	153.10	Base of strongly foliated oxide gabbro	45	280

Note: Y = yes, N = no.

**Table T2.** Curated depth to top of cored interval compared to logging depth registered from FMS data interpreted to represent oxide-bearing intervals.

Core	Depth (mbsf)	
	Curated	Correlated logging
179-1105A-		
1R	15.0	
2R	23.7	
3R	28.7	29.2
4R	33.3	34.2
5R	38.3	38.9
6R	42.8	
7R	47.8	48.3
8R	52.4	52.9
9R	57.4	57.8
10R	62.0	62.8
11R	67.0	67.8
12R	71.3	72.0
13R	76.3	76.7
14R	81.0	
15R	86.0	86.3
16R	90.6	91.3
17R	95.6	95.8
18R	100.2	101.2
19R	105.2	105.7
20R	109.8	
21R	110.8	111.0
22R	115.1	115.2
23R	119.4	119.4
24R	124.4	124.7
25R	129.0	129.3
26R	134.0	134.1
27R	138.7	138.7
28R	143.7	143.7
29R	148.4	148.6
30R	153.4	